Journal of Physics: Theories and Applications E-ISSN: 2549-7324 / P-ISSN: 2549-7316
J. Phys.: Theor. Appl. Vol. 7 No. 2 (2023) 124-138 doi: 10.20961/jphystheor-appl.v7i2.70536

Identification of sea breeze front (SBF) characteristics in the dry season using doppler weather radar on the west coast area of south Sulawesi

Nelly Handayani[1], Hasti Amrih Rejeki[2]

[1]Beringin Meteorological Station, North Barito

[2]Indonesian School of Meteorology Climatology and Geophysics, Jakarta

*Corresponding Author: nhandayani8@gmail.com

Received 27 January 2023, Revised 27 July 2023, Published 30 September 2023

Abstract: Sea Breeze Front (SBF) is one of the important components of sea breeze circulation, which plays role in coastal area's atmospheric dynamics. SBF causes significant changes in temperature and humidity profiles and initiates updrafts that induce convective activity. This study aims to determine the characteristics of SBF and its impact on convection activity using Doppler weather radar on the west coast area of South Sulawesi during dry season. SBF identification utilized PPI and CMAX products to detect convective clouds and SRI to estimate rainfall intensity, then verified it using Automatic Weather Station (AWS) and Automatic Rain Gauge (ARG). SBF was generally detected at 10.30–14.30 LT with an average moving speed of 2.04 m/s. The length of SBF ranges from 15.47–21.08 km and moves inland as far as 12.57–26.09 km with 0.51–0.89 km of column depth. There was a difference in the average value of solar radiation intensity up to 106 W/m2 and 0.5°C of temperature during SBF Days. SBF caused 17 events of convective activity with a maximum reflectivity value of 42–60 dBz and 4–8 km of cloud diameter. Five out of 17 convective activities indicated the occurrence of light rain on the surface.

Keyword : convective activity, Doppler weather radar, rainfall, sea breeze front

1. Introduction

The Indonesian Maritime Continent is a tropical island country that has the second longest coastline in the world, reaching 95,181 km, where the distribution of local rainfall amounts gradually decreases as a function of coast distance (Yamanaka et al., 2018). Sea Breeze Circulation (SBC) is a mesoscale atmospheric phenomenon caused by differences in heating between land and sea during the day that plays an important role in weather and climate dynamics in the Indonesian Maritime Continent (Hadi et al., 2002). One of the important parts of SBC is the Sea Breeze Front (SBF), which is the forefront of the sea breeze circulation that is associated with sharp changes in temperature and humidity profiles, marking the intrusion of wind flows from the sea and

creating areas with upward vertical air currents marked with the formation of cumulus clouds (Cu) during sunny weather (Miller et al., 2003).

When the SBF propagates towards land areas, convergence in front of the SBF along with increased humidity from the sea can induce convection (Suresh, 2007). If the sea breeze converges with other winds from different directions, a sea breeze front will form, which can cause the formation of local clouds and rain (Tjasyono and Harijono, 2006). When the SBF encounters other weak echoes in a parallel direction, it will cause the formation or strengthening of convective activity. According to Simpson et al. (2007), convective activity caused by SBF accounts for around 70–80% of total rainfall during the southwest monsoon season.

During the southwest monsoon, SBF is easily visible in radar images as a thin line with a reflectivity value of 13–19 dBz (Simpson et al., 2007). Suresh (2007) used Doppler weather radar to detect SBF with Plan Position Index (PPI) or Constant Altitude Plan Position Index (CAPPI) product to obtain SBF characteristics such as frequency of occurrence, onset time, intrusion into the land, length, column depth, and propagation on the surface. Hadi (2002) provides a clear definition of the SBF's presence on Jakarta's north coast during the dry season. According to Meilusiani (2018), many SBFs were detected during the dry season period within one year of the study.

The South Sulawesi region is perfectly situated for the circulation of both sea and land breezes because it is directly bordered by the Flores Sea to the south and the Makassar Strait to the west. The west coast area of South Sulawesi is included in the Doppler weather radar observation area, which is 10 km from the coast, so that research on SBF can be carried out. This study is only focused on the dry season period in order to acquire more typical SBF characteristics and learn more about convective activity that can cause severe weather.

2. Data and Methods

The research domain was on the west coast of South Sulawesi, as shown in Figure 1. The weather radar is located in Maros Regency with an observation range of 100 km, covering seven regions and cities with various lowlands and highlands. SBF research focused on the 2015–2018 dry season on the west coast of the South Sulawesi region, which is dominated by the ZOM 288 region, where the lowest rainfall occurred in the months of June, July, and August (BMKG, 2018). The data used in this study include (i) raw data volumetric extension Doppler weather radar from Hasanuddin Meteorological Station, (ii) Hasanuddin Meteorological Station's surface observational data, including temperature and solar radiation intensity, and (iii) rainfall data every 10 minutes from Automatic Weather Stations (AWS) and Automatic Rain Gauges (ARG) along the west coast of South Sulawesi, including Hasanuddin Meteorological Station AWS, Maros Climatology Station AWS, Paotere Maritime AWS, Minatasene ARG, Panaikang ARG, Gowa ARG, and Pattalasang ARG.

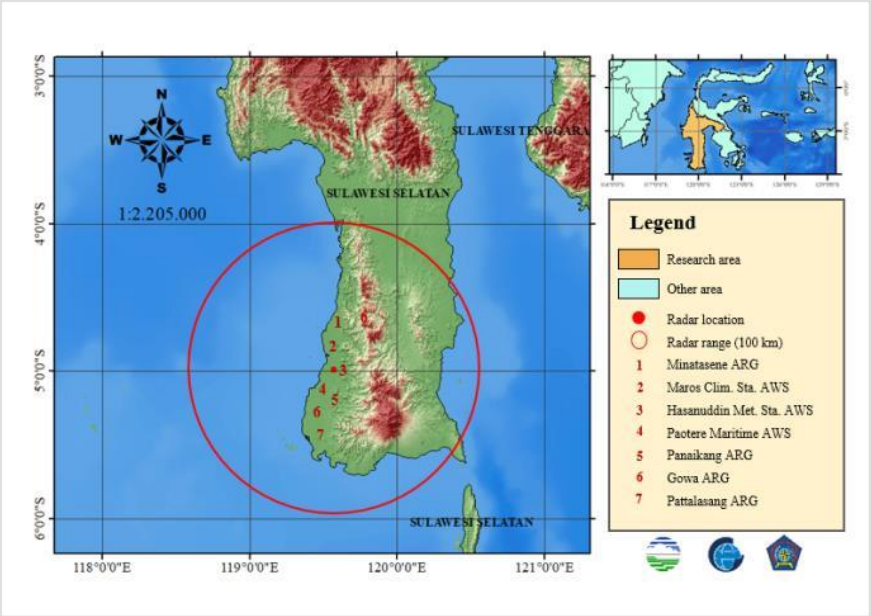

Figure 1. Research domain

The process was divided into two main parts: the identification of the SBF characteristics and the analysis of the convective clouds formed due to the SBF. The SBF identification process was carried out by processing volumetric radar data using the Rainbow 5.49 application with PPI product at the lowest elevation, namely 0.5º which is characterized by low echo reflectivity (5–20 dBZ) and in the shape of a thin line with a coastline-like pattern (Simpson et al., 2007). Figure 2 displays Makassar weather radar observations at a range of 100 km, showing limitations in the form of ground clutter (pink and green) at 0.5° elevation, interference (gray), and beam blocking (white) caused by the existence of a plateau area that extends on the east side, thus blocking radar transmissions. Due to the radar limitation, it was difficult to observe SBF; therefore, accuracy was required to identify SBF echoes from ground clutter based on their movement, where SBF moved while ground clutter did not.

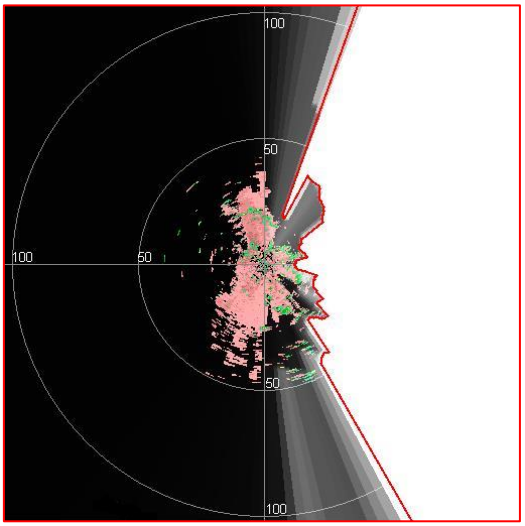

Figure 2. Makassar radar clutter at 0.5° elevation

The characteristics of the SBF were determined based on the onset time when the SBF appears. Based on the radar image generated by the PPI product, the frequency and duration of the SBF were determined. The farthest distance of the SBF intrusion to the mainland was calculated from the coastline until it started to disappear on land using the distance measurement feature. MLVCUT product was used to obtain a vertical sectional view of the SBF column depth. The SBF movement speed was calculated by dividing the intrusion distance by the duration. Furthermore, the number of occurrences, onset time, duration, intrusion distance, speed, length, and column depth were also processed as part of the frequency distribution diagram processing for each SBF parameter and divided into several class intervals. Based on the method of Sturges (1926), class intervals are calculated and then presented as a bar chart to show variation and frequency. Equation 1 describes the process for determining the class interval.

$$Intervals = \frac{range}{number\ of\ classes} \quad (1)$$

Range is the difference between the highest and lowest data value, and the number of classes (k) is calculated using Equation 2.

$$k = 1 + 3{,}3 \log n \quad (2)$$

n: amount of data

To find out the relationship between SBF and meteorological conditions, temperature and solar radiation intensity data were used on days with and without SBF. The average solar radiation intensity and temperature changed significantly on days with SBF occurrences; however, the Mean Sea Level Pressure (MSLP) value did not change much (Anjos and Lopes, 2018).

The second step involved detecting convective cloud parameters, which involved utilizing the CMAX product to calculate the maximum reflectivity value, determining the length of the cloud diameter using the distance measurement feature, and processing the radial velocity using the HWIND product to determine the wind profile horizontally when convective clouds were formed. Furthermore, the PPI product was shown alongside horizontal wind data in a single image display (overlay).

Rainfall estimation data was processed using SRI products with default settings based on Tsanyfadhila (2015), where the estimated rainfall values show better and more accurate results when using SRI products. After that, the SRI product was converted into a PAC product and modified at hourly intervals to allow for rainfall accumulation. The PAC product was then reduced to Point Rainfall Tracking (PRT) product, where the PRT product functioned to extract rainfall data at the desired location. The location in question was the location of the convective clouds induced by SBF and the nearest AWS/ARG location point to find out the estimated occurrence of rain on the surface. The rainfall verification of the radar product used AWS/ARG data that was close to the location of the convective cloud formation caused by SBF. The verification was limited

to the presence or absence of rain on the surface in the area around the formed convective clouds.

3. Results and Discussion

Based on the processing of 264 days data during the dry season in 2015, 2016, and 2018, 58 SBF occurrences were identified. The results of the SBF identification during 2017 in Makassar were carried out by Meilusiani (2018) and obtained 29 SBF occurrences, of which 20 SBF occurred during the dry season. This underlies further research, which was only focused on the dry season period in June, July, and August because other months were considered insignificant. Thus, a total of 78 SBF occurrences were observed by radar instruments during 2015, 2016, 2017, and 2018 dry season periods.

According to Holleman et al. (2006), limitations in radar observations can occur when the radar beam is completely or partially blocked by plateaus or mountains, causing limitations in the radar's ability to transmit the beam. When the radar is used for the lowest elevation observations, the radar data can be disturbed by ground clutter. The existence of limitations on the Makassar radar makes the SBF identification process quite difficult to carry out because of the presence of clutter at low elevations around the radar, and there is also a plateau that extends to the east of the radar, causing limitations in radar scanning. Figure 3 shows the results of SBF observations using PPI products at the lowest elevation. It can be seen that a thin echo resembling a coastline with a weak reflectivity value (5–20 dBZ) enters the mainland at 11.10 LT and remains there until 13.40 LT, when it becomes extinct.

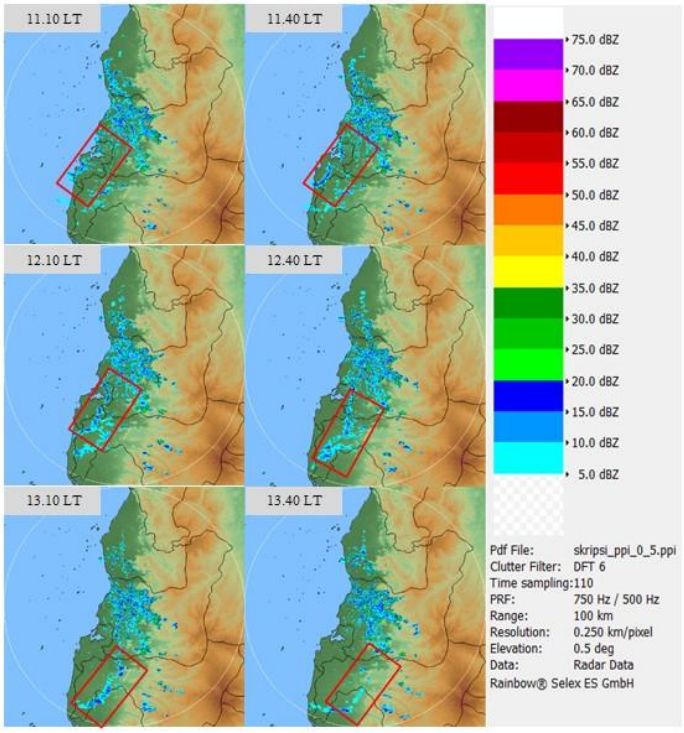

Figure 3. Identification of SBF on 02 July 2015

3.1 Identification of SBF characteristics

3.1.1 Onset time and SBF duration

SBF onset time is the moment when radar detects it for the first time as it approaches the mainland. The frequency distribution of SBF onset time in this study is shown by the graph in Figure 4(a). According to the sea breeze's intrusion period, which is a few hours after sunrise (Tjasyono and Harijono, 2013), SBF commonly appeared between 10.30 and 14.30 LT. The earliest appearance of SBF on the west coast of South Sulawesi was detected at 09.31–10.30, and the latest appearance occurred at 15.31–16.30 LT.

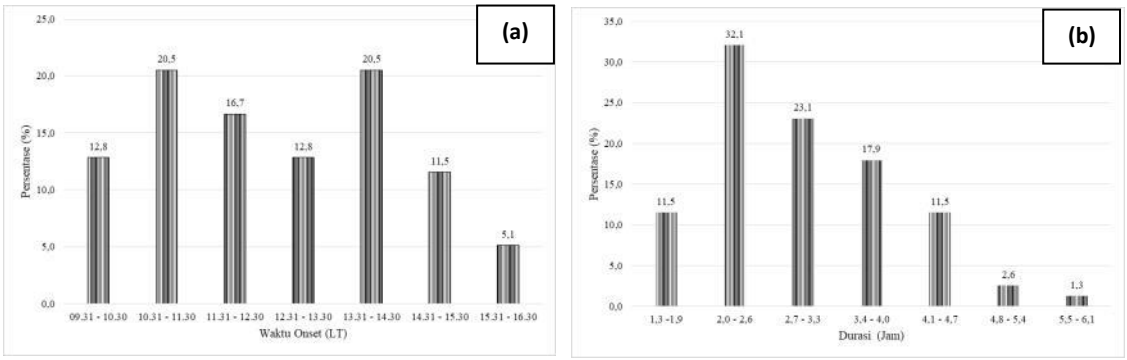

Figure 4. Frequency distribution of (a) SBF onset time, (b) SBF duration

SBF duration is the length of time it takes for SBF to evolve from onset until it eventually becomes extinct. The SBF duration would have a different value at each time and location of the occurrence. The graph in Figure 4(b) shows the frequency distribution of the SBF duration during the study period; the shortest duration of SBF was in the range of 1.3–1.9 hours, while the longest duration was 5.5–6.1 hours. The time taken by the SBF from entering land until it became extinct was 2–4 hours.

3.1.2 SBF intrusion

SBF intrusion is defined as the farthest distance of SBF when it moves to the mainland until it finally becomes extinct. According to Figure 5(a), SBF intrusion measurements were taken between the first onset position and the end SBF location utilizing the distance measurement feature on PPI products. SBF moves farther inland during the late dry season due to the higher difference in temperature between land and sea (Planchon et al., 2006). Based on the graph in Figure 5(b), SBF could move to the mainland as far as 12.57–26.09 km. The shortest distance from the SBF intrusion was in the range of 3.55–8.05 km, while the longest distance was 30.61–35.11 km. The majority of SBF intrusion on South Sulawesi's west coast moved from west to east; however, due to highland areas, SBF movement to the east was limited, and the SBF would become extinct after contacting the area.

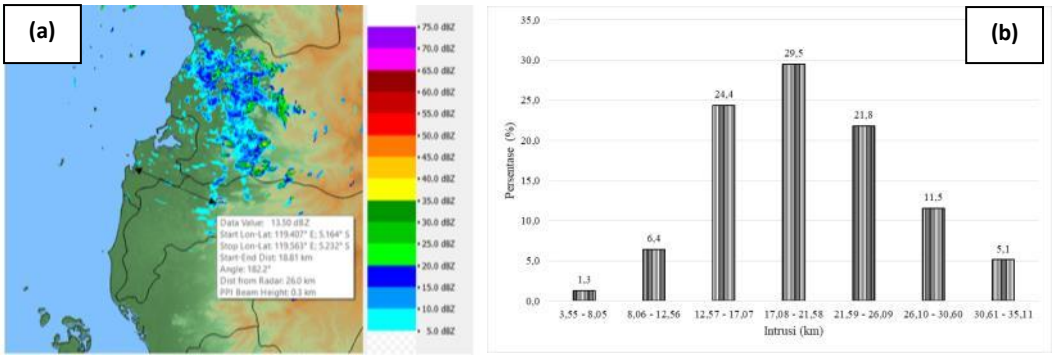

Figure 5. (a) Measurement of SBF intrusion using the distance measurement feature on 04 July 2016 at 13.40 LT, (b) SBF intrusion frequency distribution

3.1.3 SBF Length

The SBF length can be determined by measuring the distance between the two ends of the SBF using the distance measurement feature on the PPI product, as shown in Figure 6(a). The SBF in this study which was the longest and had the lowest frequency was measured in the 26.71–29.51 km range. Based on the graph in Figure 6(b), the dominant SBF length on the west coast of South Sulawesi was 15.47–21.08 km. According to Suresh (2007), the longer the SBF, the bigger the coverage area of sea breeze circulation, and thus has a greater influence.

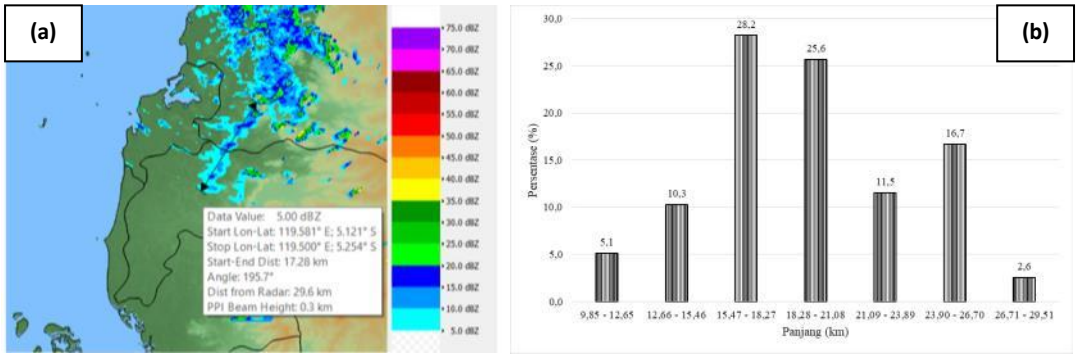

Figure 6. (a)Measurement of the SBF length using the distance measurement feature on 04 July 2016 at 13.40 LT, (b) SBF length frequency distribution

3.1.4 SBF column depth

The SBF column depth is defined as the vertical height of SBF when it moves to the mainland area. The determination of column depth in this study used MLVCUT product by following the SBF pattern formed based on the results of data processing using PPI product. Figure 7(a) displays a vertical cross-section of the SBF with the beginning point closest to the radar, representing the measurement of the SBF column depth from the MLVCUT product.

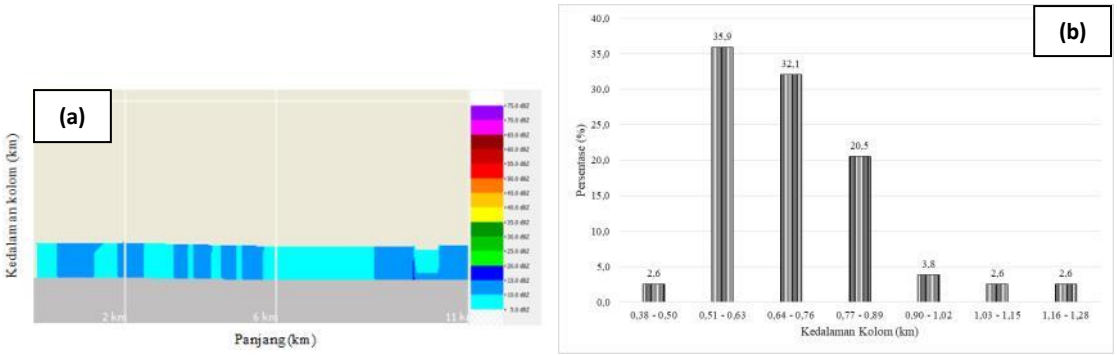

Figure 7. (a) Measurement of the SBF column depth using distance measurement feature on July 4, 2016, at 13.40 LT, (b) SBF column depth frequency distribution

Figure 7(b) depicts the frequency distribution of the SBF column depth, with the dominant column depth on South Sulawesi's west coast ranged from 0.51 to 0.89 km. According to Bhaskara et al. (1984), the depth of the sea breeze circulation is approximately 500 m, though it can exceed 1000 m. Relative humidity rises and temperature falls with increasing depth (Wexler, 1946).

3.1.5 SBF movement speed

SBF speed is defined as the magnitude of the SBF horizontal movement, as stated in m/s (Anjos and Lopes, 2018). The calculation of SBF movement speed was determined by dividing the intrusion distance by the duration that has been previously obtained using PPI products. During the study period, speed calculations were performed on all SBFs in order to obtain more accurate SBF speed characteristics. The value of the SBF movement speed on the west coast of South Sulawesi was quite varied and occurred mostly in the range of 1.1–3.5 m/s, as shown by the frequency distribution of SBF speed in Figure 8(a).

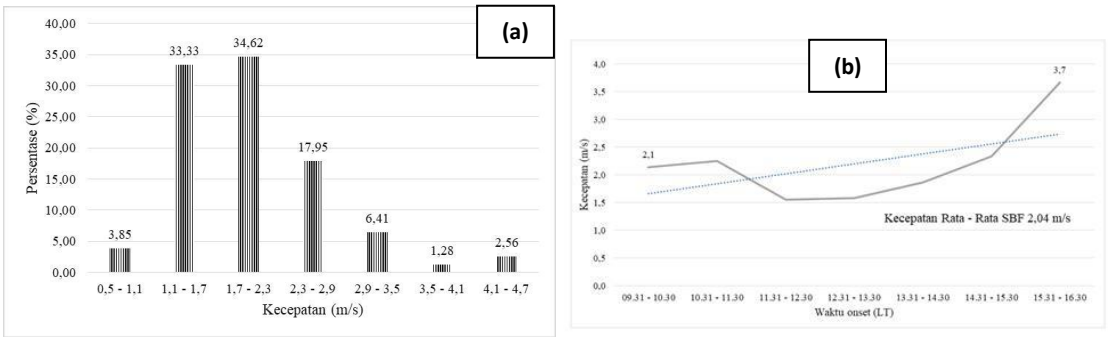

Figure 8. (a) SBF movement speed frequency distribution, (b) SBF movement speed against time graph

The average speed of SBF movement during the study period is shown in Figure 8(b), which was 2.04 m/s, where the speed of SBF increases linearly with the time of onset. In general, the average speed of SBF rises over time and reaches a maximum value when the difference between land and sea temperature reaches a maximum

(Tjasyono, 2008). The maximum average speed value on the west coast of South Sulawesi occurred at the time of the latest onset, i.e., 3.7 m/s. Due to the increasing temperature difference between land and sea, the SBF is moving at an increased rate.

3.2 Analysis of meteorological conditions during the SBF occurrences

The parameters for analyzing meteorological conditions used in this study were temperature and solar radiation intensity. These meteorological conditions were further divided into two categories: conditions on days where there were SBF occurrences (SBF days) and conditions on days without SBF occurrences (non-SBF days) throughout the study period. During the study period, 78 days had SBF occurrences, while the number of days without SBF occurrence was 271. The average solar radiation intensity on SBF days was 1890 W/m^2, greater than the average on non-SBF days, which was 1784 W/m^2, with a difference of up to 106 W/m^2. This indicated that SBF occurs in conditions that tend to be warmer. The graph of the temperature difference between SBF days and non-SBFs day is shown in Figure 9.

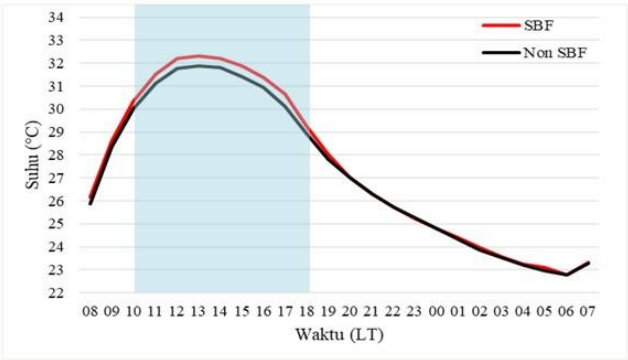

Figure 9. Comparison of SBF day and non-SBF day temperatures

Based on Figure 9, the temperature parameters basically have a similar pattern, both on SBF days and non-SBF days. The blue area in Figure 9 shows the temperature value when the SBF time range was detected based on the characteristics obtained in the previous sub-chapter, namely from 01.40 UTC to 10.00 UTC, where the difference in temperature values was visible at that time. The temperature during the SBF day had a higher value compared to the non-SBF day, with a difference in value of 0.5°C. When SBF occurs, sky conditions tend to be clear so that direct solar radiation into the lower atmosphere causes the available energy to be converted into sensible heat flow, which increases temperature and produces warmer days (Anjos and Lopes, 2018).

3.3 SBF-induced convective activity

The convective activity caused by SBF on the west coast area of South Sulawesi was induced by the convergence that occurs when SBF encounters other echoes in the opposite direction, according to research conducted by Yan et al. (2012) using the HWIND product. The results of the HWIND product overlay with the PPI product

output were used to see the horizontal wind profile, as shown in Figure 10 in the red box area.

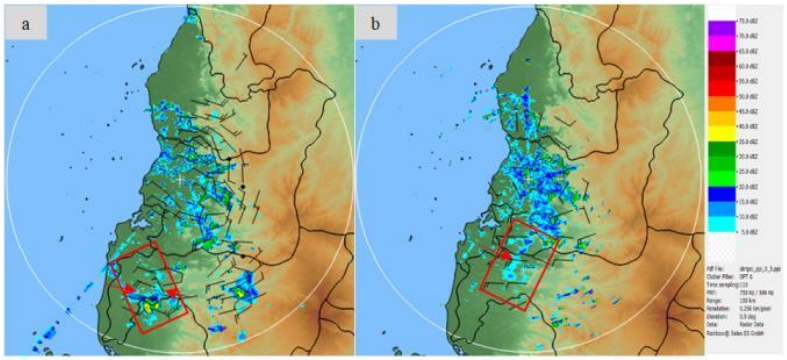

Figure 10. Horizontal wind profile (a) SBF initiates convective activity on June 1, 2018; (b) SBF does not initiate convective activity on July 4, 2016.

Figure 10 (a) depicts the convergence of the SBF coming from the sea and other echoes coming from other directions, where the SBF originated from the west and other echoes originated from the east, causing convergence. Convective activity could be brought on by this convergence occurrence. The SBF was moving from the west in Figure 10(b), and as there were no echoes coming from any other directions, convective activity was not induced.

According to Simpson (1994), SBF is related to the penetration of sea breeze towards the land, which forces warmer and unstable land air masses to rise in front of the sea breeze circulation, causing condensation to occur and forming clouds. Based on the reflectivity value generated by the CMAX product, the strength of the convective activity can subsequently be determined. The reflectivity value in the active convective phase is more than or equivalent to 38 dBZ, according to Gamache and Houze (1982).

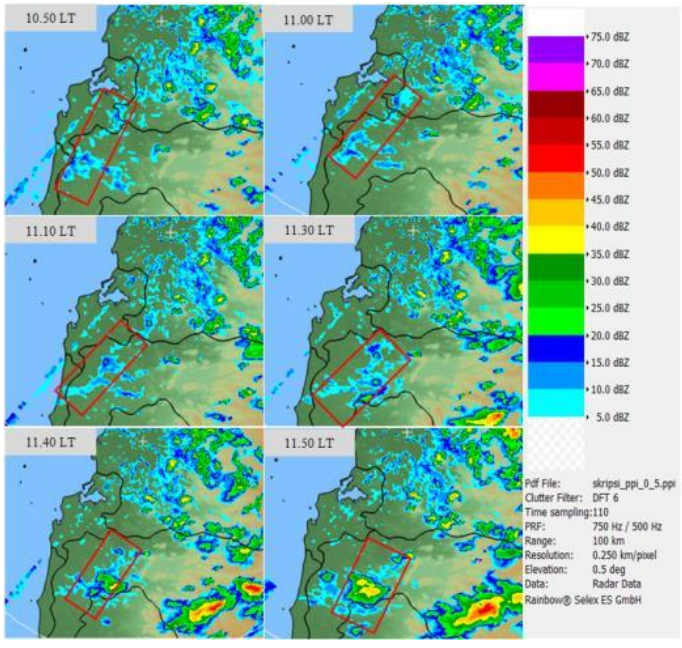

Figure 11. SBF-induced convective activity on June 12, 2018

Convective activity caused by SBF is characterized by the growth of convective clouds near the SBF location, both while it is still present and after the SBF has disappeared, as shown in Figure 11. Convective clouds formed just before SBF became extinct at 11.40 LT. The convective activity could be identified using the CMAX product to obtain the maximum reflectivity value, while the distance measurement feature was used to determine the diameter of the convective clouds that formed. 78 SBF occurred in the west coast region of South Sulawesi during the study period, with 21.8% causing convective activity and 78.2% not.

Table 1. Convective cloud growth identification results

No.	Date	Reflectivity (dBZ)	Diameter (km)
1.	2016/06/12	42.5	6.71
2.	2016/06/18	56.5	6.84
3.	2016/06/19	51	8.06
4.	2016/06/22	52	8.2
5.	2018/06/01	50.5	4.03
6.	2018/06/02	51.5	4.51
7.	2018/06/12	43.5	3.04
8.	2018/06/14	48	4.65
9.	2018/08/09	56	4.61
10.	2018/08/10	52.5	4.16

The identification parameters for convective clouds used in this study were the reflectivity value and cloud diameter. According to Table 1, the diameter of the convective cloud and the maximum reflectivity vary with each event. Convective clouds were formed, with reflectivity values ranging from 42 to 60 dBz and diameters ranging from 3 to 8 km. The maximum reflectivity value of the largest convective cloud was 56.5 dBZ, and the largest diameter reached 8.2 km. Convective clouds induced by SBF occurrences are single cell type convective clouds, according to research done by Novitasari (2017).

3.4 Rainfall due to convective activity induced by SBF

Precipitation caused by convective activity from SBF can be predicted using the Z–R radar equation by Suresh (2007). Based on verification work done by Tsanyfadhila (2015), SRI products are utilized with default settings to estimate rainfall for Makassar and the surrounding area. The estimated rainfall values indicate better and more accurate results when utilizing SRI products compared to other radar hydrological products. The PAC product then estimated the value of the accumulated rainfall using the result of the SRI product as input data. In order to process the estimated rainfall data, PRT products were used. These products were processed at two points: the convective cloud location point and the AWS/ARG location point. The processing of

rain estimation at cloud locations was intended to find out how much rainfall could occur on the surface due to the presence of convective clouds induced by SBF. If the location of the convective clouds did not coincide with the location of the rain gauge, then the processing of the estimated rainfall was also carried out at the nearest AWS/ARG point, and thus the results of the estimation could be verified against the results of the rainfall detected by the rain gauge on AWS/ARG. The verification of the rainfall in question was limited to the existence or absence of rain on the surface in the area around the formed convective clouds. Table 2 displays the estimated rainfall for each convective cloud.

Table 2. Estimated rainfall results

Date	Reflectivity (dBZ)	Convective cloud location	Gauge location	Distance (km)	Rainfall (mm)		
					CE	GE	AWS/ ARG
2016/06/12	42.5	119.42 E 5.27 S	Gowa ARG	12.1	1.6	0	0
2016/06/18	56.5	119.49 E 5.33 S	Pattalasang ARG	8.9	13.0	TTU	0
2016/06/19	51	119.55 E 5.22 S	Gowa ARG	1.9	8.3	0.2	0
2016/06/22	52	119.39 E 5.32 S	Pattalasang ARG	10.1	18.3	1.7	1.4
2017/06/05	50	119.38 E 5.36 S	Pattalasang ARG	8.76	1.4	TTU	0
2017/06/07	60	119.54 E 5.09 S	Panaikang ARG	5.1	1.2	TTU	0
2017/06/14	50	119.44 E 5.27 S	Gowa ARG	11.5	2.0	TTU	0
2017/06/15	60	119.39 E 5.36 S	Pattalasang ARG	6.9	4.8	TTU	0
2017/06/16	50	119.43 E 5.22 S	Panaikang ARG	9.8	0.6	0	0
2017/06/18	50	119.41 E 5.39 S	Pattalasang ARG	2.4	5.0	TTU	0
2017/08/02	60	119.43 E 5.11 S	Paotere AWS	0	1.8	1.8	1.2
2018/06/01	50.5	119.49 E 5.23 S	Pattalasang ARG	10.5	1.2	0	0
2018/06/02	51.5	119.47 E 5.12 S	Paotere AWS	0	10.8	10.8	8.1
2018/06/12	43.5	119.50 E 5.28 S	Gowa ARG	10.2	1.0	0.2	0
2018/06/14	48	119.45 E 5.14 S	Panaikang ARG	0	3.2	3.2	0.8
2018/08/09	56	119.52 E 5.27 S	Gowa ARG	7.3	1.4	TTU	0
2018/08/10	52.5	119.47 E 5.21 S	Gowa ARG	3.8	3.4	4.5	2.7

CE: estimated rainfall at the location of convective clouds
GE: estimated rainfall at the AWS/ARG location
TTU: immeasurable

Based on Table 2, the distance between the convective clouds and the AWS/ARG locations ranges from 0 to 12 km. Three out of a total of 17 occurrences—on August 2, 2017, as well as June 2 and 14 of this year—had convective cloud locations that coincided with the AWS/ARG sites. It is possible to directly verify the outcomes of radar-estimated rainfall using rain gauges on AWS/ARG due to the location's appropriateness. On August 2, 2017, SBF-initiated convective clouds formed directly above Paotere Maritime AWS, with estimated rainfall of 1.8 mm and actual AWS observations of 1.2 mm. The estimated rainfall for the convective activity that formed at the Paotere Maritime AWS site on June 2, 2018, was 10.8 mm, while the actual rainfall measured by AWS was 8.1 mm. The results of the estimated rainfall on June 14, 2018 from the convective clouds that formed at the Panaikang ARG site were 3.2 mm, while the results of rainfall measurements at AWS were 0.8 mm. Based on these three cases, convective clouds that are near AWS/ARG can induce rainfall on the surface. Only two of the 14 convective activities whose locations do not coincide with AWS/ARG caused rain on the surface: on June 22, 2016 and August 10, 2018. Based on Table 2, the convective cloud diameter was 8.2 km with a reflectivity value of 52 dBZ and 10.1 km from Pattalasang ARG. The estimated rainfall at the cloud's location was 18.3 mm, while the estimated amount at the ARG site was 1.7 mm and the actual amount of precipitation at the ARG was 1.4 mm. The convective clouds that formed on August 10, 2018, had a diameter of 4.16 km, a reflectivity of 52.5 dBZ, and were located 3.8 km from Gowa ARG. While the measured rainfall at ARG is 2.7 mm, the estimated rainfall at cloud locations was 3.4 mm and at ARG sites was 4.5 mm.

Convective clouds caused by SBF can produce rainfall on the surface during the dry season, according to Simpson et al. (2007). Based on the results of rainfall estimation using the Z–R radar equation, rainfall was predicted to occur in all convective activity induced by SBF; however, not all can be verified using AWS/ARG due to the considerable distance. Out of a total of 17 convective activities that occurred, 5 cases resulted in rain with a light intensity on the surface and were successfully verified by the nearest AWS/ARG.

4. Conclusion

The Sea Breeze Front detected on the west coast of South Sulawesi during the 2015–2018 dry season generally comes from the west with an average movement speed of 2.04 m/s. Most SBF onset times occur between 10.30 and 14.30 LT and last for 2–4 hours. The length of the SBF is in the range of 15.47–21.08 km, with an intrusion distance of 12.57–26.09 km. Due to the existence of a highland area, the SBF's movement to the east is limited, and once it approaches the area, it will become extinct. The measured SBF column's depth ranges from 0.51 to 0.89 kilometers. During the dry season of 2015–2018, SBF can induce convective activity as much as 21.8% of 78 occurrences, with maximum reflectivity values reaching 42–60 dBz and cloud diameters of 4–8 km. Five out of 17 convective activities initiated by SBF can cause light rainfall on the west coast of South Sulawesi.

References

Anjos, M. and A. Lopes. (2018). Sea breeze front identification on the north eastern coast of Brazil and its implications for meteorological conditions in the Sergipe region. *Theoretical and Applied Climatology*, *137*, 2151–2165.

BMKG. (2018). *Prakiraan Musim Hujan 2018/2019 di Indonesia*. Jakarta, ID: Badan Meteorologi Klimatologi dan Geofisika.

Bhaskara, N.S., S. D. Williams, M. Chandy, and U. Devi. (1984). Study of sea breeze at Madras. *Mausam*, *35*, 537–538.

Gamache, J. F. and R. A. Houze Jr. (1982). Mesoscale Air motions Associated with a Tropical Squall Line. *American Meteorology Society, 110,* 118–135.

Hadi, T. W., T. Horinouchi, T. Tsuda, H. Hashiguchi, and S. Fukao. (2002). Sea–Breeze Circulation over Jakarta, Indonesia: A Climatology Based on Boundary Layer Radar Observations. *Monthly Weather Review*, *130*, 2153–2166.

Holleman, I., D. Michelson, G. Galli, U. Germann and M. Peura. (2006). *Quality Information for Radars and Radar Data.* EU: OPERA Workpackage, Europe.

Meilusiani, T. C. (2018). Identifikasi Karakteristik Sea Breeze Front dan Pengaruhnya Terhadap Aktivitas Konvektif di Makassar Tahun 2017 Menggunakan Radar Cuaca Doppler. Jakarta, ID: Sekolah Tinggi Meteorologi Klimatologi dan Geofisika.

Miller, S. T. K., B. D. Keim, R. W. Talbot, and H. Mao. (2003). Sea Breeze: Structure, Forecasting, and Impacts. *Reviews of Geophysics*, *41*(3), 1–30.

Novitasari, A. S. (2017). Karakteristik Sea Breeze Front dan Kaitannya Terhadap Aktivitas Konvektif di Pantai Utara Jakarta. Jakarta, ID: Sekolah Tinggi Meteorologi Klimatologi dan Geofisika.

Planchon, O., F. Damato, V. Dubreuil, and P. Gouery. (2006). A Method of Identifying and Locating Sea–Breeze Fronts in North–Eastern Brazil by Remote Sensing. *Meteorology Appl.*, *13*, 225–234.

SELEX. (2013) S*oftware Manual Rainbow 5 Product & Algorithms.* Neuss, DE: SELEX SIGmbH.

Simpson, J. E. (1994) *Sea Breeze and Local Wind*. Cambridge, GB: Department of Applied Mathematics and Theoretical Physics University of Cambridge.

Simpson, M., H. Warrior, S. Raman, P. A. Aswathanarayana, U. C. Mohanty, and R. Suresh. (2007). Sea–Breeze–Initiated Rainfall Over The East Coast of India During The Indian Southwest Monsoon. *Journal of the International Society for the Prevention and Mitigation of Natural Hazards*, *42*(2), 401–413.

Sturges, H.A. (1926). The Choice of a Class Interval. *Journal of the American Statistical Association*, *21*(153), 65–66.

Suresh, R. (2007). Observation of sea Breeze Front and Its Induced Convection Over Chennai in Southern Pennisular India Using Doppler Weather Radar. *Pure and Applied Geophysics*, *164*, 1511–1525.

Tjasyono, B. (2008). *Sains Atmosfer*. Jakarta, ID: Badan Meteorologi Klimatologi dan Geofisika.

Tjasyono, B. and S. W. Harijono. (2013). *Atmosfer Ekuatorial*. Jakarta, ID: Badan Meteorologi Klimatologi dan Geofisika.

Tsanyfadhila, S. (2015). Kajian Produk Radar untuk Estimasi Curah Hujan di Makassar dan Sekitarnya. Jakarta, ID: Sekolah Tinggi Meteorologi Klimatologi dan Geofisika.

Yamanaka, M.D., S. Ogino, P. Wu, H. J. Ichi, S. Mori, J. Matsumoto, and F. Syamsudin. (2018). Maritime Continent Coastlines Controlling Earth's Climate, *Progress in Earth and Planetary Science*, *5*(1).

Yan, W., Y. Lili, and Z. Nannan. (2012). Sea Breeze Front and Convective Weather Events Detected by Doppler Weather Radar. *International Congress on Informatics, Environment, Energy and Applications*.

Wexler, R. (1946). Theory and Observations of Land and Sea Breezes. *Bulletin American Meteorological Society, 27*, 272–287.